On the Influence of Transducer Internal Loss in Piezoelectric Energy Harvesting with SSHI Interface

J. R. LIANG AND W. H. LIAO*

Smart Materials and Structures Laboratory, Department of Mechanical and Automation Engineering
The Chinese University of Hong Kong, Shatin, N. T., Hong Kong, China

ABSTRACT: In piezoelectric energy harvesting, the harvesting efficiency can be greatly improved with the switching interface called synchronized switch harvesting on inductor. However, we found from experiments that, the voltage across the piezoelectric element reverses a little bit after every inversion. This reversion, although small compared to the inversion, weakens the inversion effect produced by the switching inductive shortcut, and therefore decreases the voltage magnitude as well as the harvesting efficiency a lot. This phenomenon can also be found from the experimental waveforms in the previous studies; but it has never been pointed out. In these studies, the analytical results, which used the measured effective inversion factor in calculation, agreed with experiments; yet, the origin of the reversion after every switching action, as well as the quantitative relation between the ideal and effective inversion factors are of interest. In this article, the phenomenon on voltage reversion after every inversion is first described. Based on the experimental results, it is analyzed that this reversion is caused by the transducer internal loss. A revised model considering the influence of the internal energy loss is introduced. With this model, not only the reason, which causes the reversion after every inversion, can be explained; but also the quantitative relation between the ideal and effective inversion factors can be obtained. Experiments are also conducted to validate the revised model.

Key Words: piezoelectric, energy harvesting, transducer loss, dielectric loss, SSHI.

INTRODUCTION

UBIQUITOUS deployed sensor networks and mobile electronics are the most potential applications, which might gain benefit from the development of energy harvesting (also known as power harvesting and energy scavenging; Sodano et al., 2004; Paradiso and Starner, 2005; Anton and Sodano, 2007). In these fields, until now, most of the devices are powered by batteries. Due to batteries' capability in energy storage, these devices inevitably face the problems on limited lifetime and bothering replacement or recharging for batteries. On the other hand, instead of installing batteries to store enough energy to power these autonomous devices over a long working period, energy might be continually obtained from ambient sources (e.g., solar power, thermal energy, wind energy, and vibration energy) by equipping with small energy harvesters.

Piezoelectric energy harvesting (PEH) is one of the promising techniques that can scavenge energy from ambient vibration sources. With its electromechanical coupling characteristic, a piezoelectric element can generate electricity when strain is induced. Since the deformation in vibrating structures is alternating, the generated electricity is also alternating. An interface circuitry is needed for AC–DC conversion. The standard energy harvesting (SEH) interface involves only a bridge rectifier for the AC–DC conversion (Ottman et al., 2002). To further improve the energy harvesting efficiency, Guyomar et al. (2005) proposed a treatment named synchronized switch harvesting on inductor (SSHI). It was claimed that, under the same displacement excitation, SSHI can increase the harvested power by several hundred percents, compared to SEH. The improvement would be more significant for weakly coupled PEH systems (Shu et al., 2007).

The inversion factor γ plays an important role in the SSHI treatment. Theoretically, under displacement excitation, the harvesting power can reach infinity when γ approaches -1 (Lefeuvre et al., 2006).[1] In addition, the effective inversion was regarded to be only related to the quality factor of the switching RLC loop. Yet, in experiment, since a voltage reversion is found right after every voltage inversion across the piezoelectric element. The effective inversion factor in fact is always larger than the

*Author to whom correspondence should be addressed.
E-mail: whliao@cuhk.edu.hk
Figure 8 appears in color online: http://jim.sagepub.com

[1]The inversion factor γ in this article is defined in Equation (3). The sign information is also included here. It is the opposite number of that given by Lefeuvre et al. (2006).

1045-389X/11/05 0503–10 $10.00/0 DOI: 10.1177/1045389X11401447

theoretical one, so that the inversion effect is weakened. It makes the practical voltage magnitude, as well as the harvesting power, much smaller than those in theoretical prediction with the ideal inversion factor. Most literatures on SSHI only emphasized its outstanding capability on enhancing the harvesting efficiency; the effective inversion factor used in calculation was obtained from measurement. This phenomenon on reversion and the difference between the ideal and effective inversion factors were ignored previously.

Given an SSHI system constructed with lossless piezoelectric element and switching path, this phenomenon cannot be explained. After investigating the waveforms in the practical SSHI circuit, we found that the reversion is attributed to the transducer energy loss, which is due to internal current leakage within the piezoelectric transducer. Besides the piezoelectric capacitance, the transducer loss is also an important electrical characteristic of piezoelectric materials in practical energy harvesting systems. But it was not considered in the PEH researches.

The purpose of this article is to provide a detailed description on the phenomenon of voltage reversion after every inversion, as well as propose a revised model to analyze the influence of the transducer internal loss in PEH with SSHI interface.

HARVESTING WITH SSHI INTERFACE

Given a typical piezoelectric device, e.g., a piezoelectric cantilever with shunt circuit, its single degree of freedom schematic representation is shown in Figure 1. Under harmonic displacement excitation, the piezoelectric element was commonly modeled as an equivalent current source i_{eq} in parallel with the piezoelectric clamped capacitance C_p (Ottman et al., 2002; Guan and Liao, 2009; Wu et al., 2009), as shown in Figure 2. i_{eq} is proportional to the velocity $\dot{x}$ with the relation of:

$$i_{eq}(t) = \alpha_e \dot{x}(t) \tag{1}$$

where α_e is the piezoelectric force–voltage coupling factor.

Different shunt circuits for different treatments were designed to extract energy from the vibrating mechanical structure. For the purpose of structural damping, the extracted energy is directly dissipated; while for energy harvesting, a portion of the extracted energy is reclaimed and stored in electrical form for subsequent usage.

In a vibrating piezoelectric element, since the induced voltage across the piezoelectric capacitance is alternating, the most conventional way to turn an AC voltage into DC is to use a bridge rectifier for rectification and then a capacitor for filtering. The combination of bridge rectifier and filter capacitor forms the standard interface

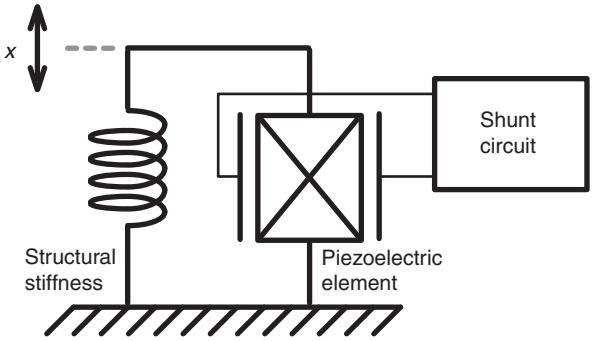

Figure 1. *Schematic representation of a typical piezoelectric device.*

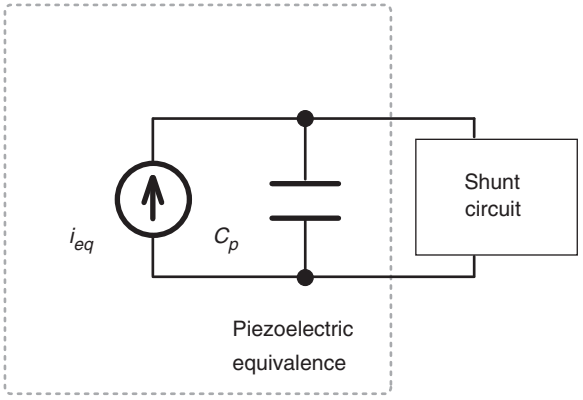

Figure 2. *Equivalent circuit of a typical piezoelectric device.*

circuit that can be used for energy harvesting, i.e., SEH. Ottman et al. (2002) discussed the optimization to the SEH technique. Yet, using SEH cannot ensure that the energy is always flowing from mechanical part to electrical part. During a certain interval in every cycle, energy returns from electrical part to mechanical part. It was called energy return phenomenon (Liang and Liao, 2009).

The SSHI treatment overcomes this problem by adding an inductive switching path to the SEH circuit. This path can be connected in parallel to the bridge rectifier to form a parallel SSHI (P-SSHI) circuit (Figure 3(a)), or in series to form a series SSHI (S-SSHI) circuit (Figure 3(b)) (Lefeuvre et al., 2006). Regardless of P-SSHI or S-SSHI, the inductive switching path switches on to form a series RLC loop once the displacement x reaches its extreme values,[2] and then switches off after half of a RLC cycle, i.e.:

$$\tau = \pi\sqrt{L_i C_p} \tag{2}$$

where L_i is the inductance in the switching shortcut, as shown in Figure 3(a) and (b). The voltage across the capacitance, denoted as v_p, inverts during the short

[2]At these very instants, the velocity $\dot{x}$ as well as the current i_{eq} cross zeros.

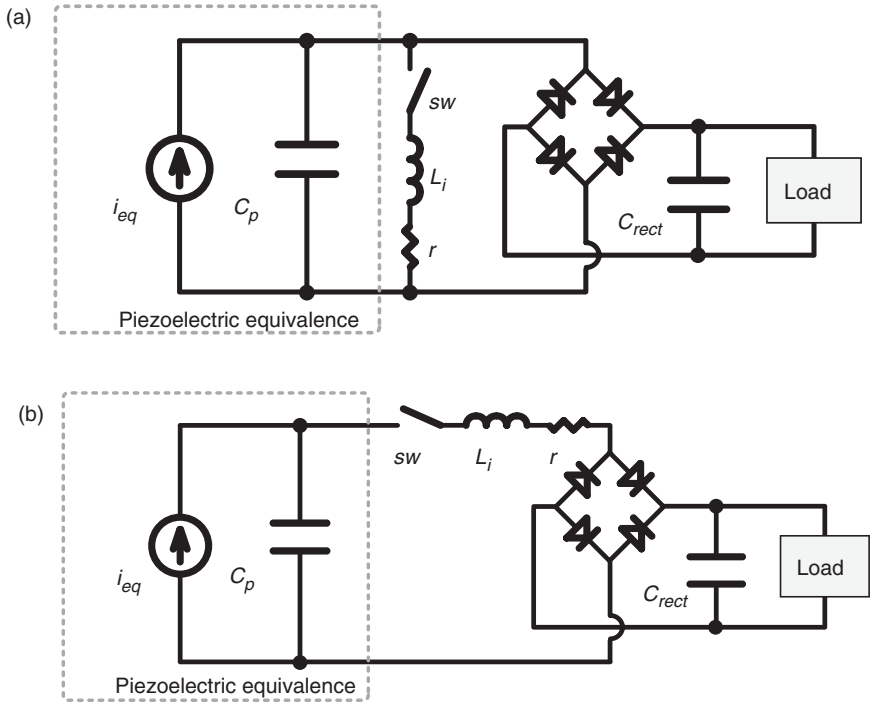

Figure 3. *Equivalent circuits of two SSHI treatments: (a) P-SSHI and (b) S-SSHI.*

interval τ, which is much smaller than the mechanical cycle, with the ideal inversion factor of:

$$\gamma = \frac{V_{off} - V_{ref}}{V_{on} - V_{ref}} = -e^{-\pi/(2Q)} \tag{3}$$

where Q is the quality factor of the RLC loop, V_{on} and V_{off} the voltages at the start and end of the voltage inversion, respectively, and V_{ref} the reference voltage in the inversion. In P-SSHI, V_{ref} equals zero; in S-SSHI, V_{ref} equals the rectified voltage V_{rect}. Typical waveforms of P-SSHI or S-SSHI as well as the zoom-in view to one of the switching processes are shown in Figure 4(a)–(c), respectively. The parameters τ, V_{on}, V_{off}, and V_{ref} are illustrated in Figure 4(c). Since i_{eq} is proportional to $\dot{x}$, these switching actions make v_p in phase with i_{eq}. It ensures that the power input from mechanical part to electrical part, which equals to the product of v_p and i_{eq}, is always positive. Moreover, the SSHI also boosts the magnitude of v_p to enable a larger power conversion.

PHENOMENON

SSHI does provide an effective mechanism to increase the harvesting energy under the same excitation level; the analytical results provided in the previous literatures matched experiments as well. However, a phenomenon observed from the experimental waveform, which differs from that in ideal one, was ignored. In this section, with the focus on the S-SSHI interface, this phenomenon will be described and analyzed in detail.

Applying a 30-Hz constant (in magnitude) displacement excitation to a piezoelectric cantilever, whose first resonance frequency is nearby, a 20-V open circuit voltage is recorded across the piezoelectric element, i.e., $V_{oc} = 20$-V. Figure 5(a) shows the voltage waveforms when S-SSHI treatment is activated under 7.6 V rectified voltage,[3] i.e., $V_{rect} = 7.6$ V. Figure 5(b) shows the zoom-in view to one of the switching instants around time origin. When the switching command is applied, the voltage level before and after the switching action can be obtained as V_{on} and V_{off}, respectively, as indicated in Figure 5(b). Given $V_{ref} = V_{rect}$ in S-SSHI, substituting the measured V_{on}, V_{off}, and V_{rect} into Equation (3) yields the ideal inversion factor of the inductive shortcut $\gamma = -0.80$. Ideally, without any loss, the effect of SSHI treatment is to, intuitively, split the open-circuit voltages at maxima and minima places and move the adjacent parts against each other to some extent. Lefeuvre et al. (2006) gave the formulas with which the S-SSHI characteristic voltage waveform can be theoretically obtained. Based on these formulas, the dot curve in Figure 5(a) shows the theoretical waveform of v_p with $\gamma = -0.80$. Nevertheless, there is a large discrepancy between the calculated result and the experimental one (gray bold curve). Two features, which differ from those

[3]The effective rectified voltage V_{rect} is the sum of V_{store} the voltage across C_{rect}, and V_F, the forward voltage gap of the bridge rectifier. V_{store} is regarded as constant during every vibration cycle, since C_{rect} is usually selected much larger than C_p. V_F is about 1.0 V in our experimental circuit.

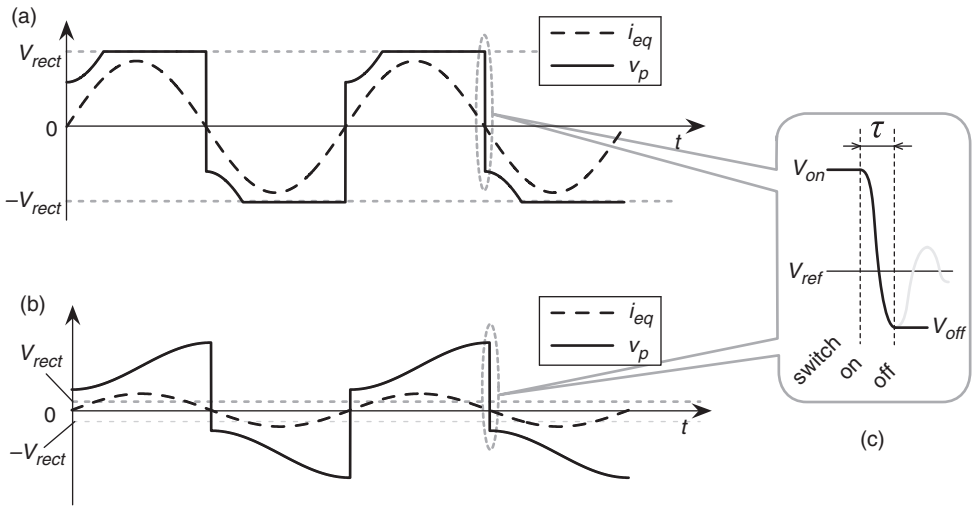

Figure 4. *Typical waveforms of two SSHI treatments: (a) P-SSHI, (b) S-SSHI, and (c) inversion of* v_p *at the instant of extreme displacements.*

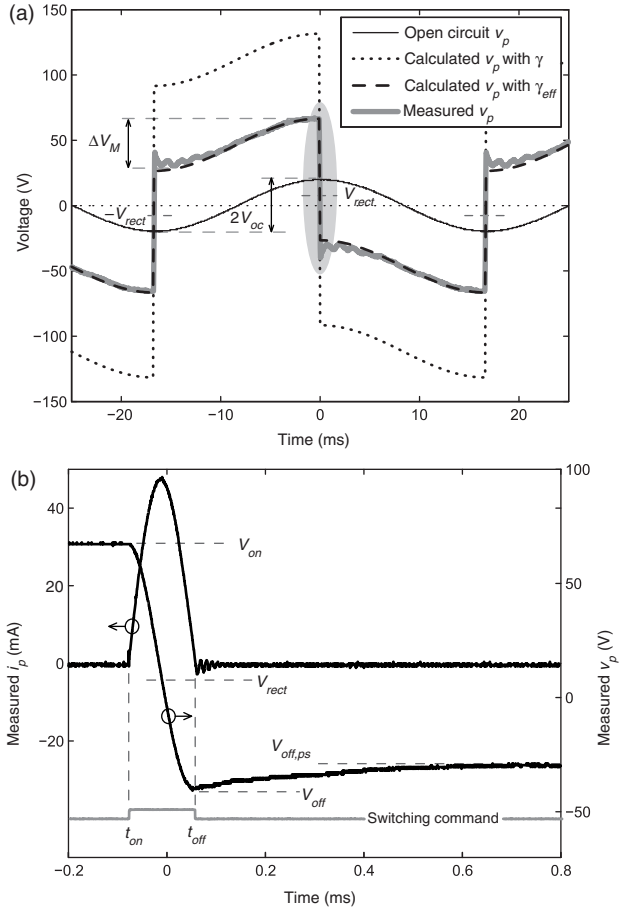

Figure 5. *Characteristic waveforms in S-SSHI* ($V_{oc}=20$ *V,* $V_{rect}=7.6$ *V): (a) voltages and (b) zoom-in view to the voltage and current around time origin.*

in theoretical waveform, can be observed from the experimental waveform:

1. As highlighted by the ellipse area in Figure 5(a), the voltage v_p reverses somewhat right after every inversion. Small damped oscillation can be observed as well.
2. The measured voltage difference between two switching instants in S-SSHI, i.e., ΔV_M, as indicated in Figure 5(a), is smaller than, rather than equals to, that in open circuit condition, i.e., $2V_{oc}$.

For the first feature, similarities can be observed from the experimental waveforms provided by Richard et al. (2000), Guyomar et al. (2006), and Lallart and Guyomar (2008). This reversion counteracts the inversion, therefore makes the effective inversion factor above the ideal inversion factor γ, implying that the inversion effect is weakened. A small reduction in the magnitude of the inversion factor usually causes large drop in the magnitude of v_p. The second feature imposes an equivalent effect so as to decrease V_{oc}, which also results in the magnitude reduction of v_p. These two features were not pointed out in the previous literatures, not to mention the origin of them. However, their theoretical results still agreed with the experiments, because, instead of using the ideal inversion factor γ in calculation, they used the effective inversion factor (denoted as γ_{eff} in the following part of this article), which can be estimated by taking the voltage level after the reversion as the pseudo V_{off}. For instance, as shown in Figure 5(a), when $\gamma_{eff}=-0.59$, the calculated waveform (dashed curve) matches the measured result. But even γ_{eff} can be approximately obtained from the experimental waveform, the reason about the voltage reversion, as well as the relation between γ and γ_{eff} are of interest.

These questions can be studied with an investigation on the voltage and current in one of the switching instants. Since v_p is proportional to the charge stored in the piezoelectric capacitance C_p, the reversion of v_p after every inversion must be resulted from some current leakage. For the observation of the instant current

flowing through the treatment circuit during the switching instant, a 10-Ω current sampling resistor is connected to the treatment circuit in series. As shown in Figure 5(b), the switch begins to conduct at t_{on}, and then is blocked at t_{off}. The current i_p approaches zero quickly after the switching path is blocked at t_{off}, in spite of some low level oscillation. However, after t_{off}, v_p keeps reversing even no current leaks through the shunt circuit.[4] Based on this observation, it can be concluded that the current leakage should take place *internally* within the piezoelectric transducer. Therefore, the voltage reversion in SSHI is caused by the internal energy loss within the piezoelectric transducer, which was not mentioned in the previous studies on PEH with SSHI.

Generally, there are three loss mechanisms in piezoelectric transducers, i.e., mechanical loss, dielectric loss, and piezoelectric loss (Umeda et al., 1998). In particular, in the studies for piezoelectric ceramics, it was reported that the influence of dielectric loss increases intensively under high-power operation (Hirose et al., 1993). Since SSHI treatment boosts the voltage level across the piezoelectric element, as well as the conversion power, it is rational that the dielectric loss might influence the harvesting system more, when conversion power is getting larger.

ANALYSIS

The conventional equivalent circuit of S-SSHI, as given in Figure 3(b), which considered the piezoelectric element as an energy lossless component, is no longer capable to show details on the mechanism of voltage reversion in S-SSHI. In this section, a new analysis based on the revised equivalent circuit is proposed, so as to evaluate the influence of transducer internal loss in S-SSHI.

Revised Model

In order to study the high-power characteristics of piezoelectric transducers, Umeda et al. (1998) proposed a comprehensive model, based on which different loss mechanisms within the transducers can be embodied and taken into consideration. The revised equivalent circuit is shown in Figure 6. In this revised equivalent circuit, the resistances R_m, R_d, and R_p represent the mechanisms of mechanical loss, dielectric loss, and piezoelectric loss, respectively.

Referring to the equivalent circuit shown in Figure 6, the equivalent circuit of S-SSHI treatment is revised and shown in Figure 7. In Figure 6, the three components of R_m, L_m, and C_m correspond to the inherent damping, mass, and stiffness in the mechanical

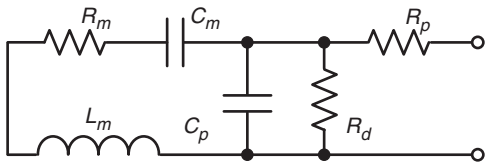

Figure 6. *Equivalent circuit including the loss mechanisms.*

domain, respectively. They together represent the dynamics of the mechanical part in the PEH system. But since constant displacement excitation is adopted in this study, which implies that the mechanical dynamics is neglected, the total effect of R_m, L_m, and C_m is substituted by an equivalent current source i_{eq}, as shown in Figure 7. Therefore, in this analysis, the influence of mechanical loss is not included.

The resistance R_p corresponding to the piezoelectric loss is in series with the parasitic resistance of the switching path, i.e., r. Their total resistance influences the Q factor of the switching RLC loop. Their effects are together embodied with the inversion factor γ; yet, the effects can be hardly separated from each other. On the other hand, larger R_p might lower the magnitude of voltage inversion. But this equivalent series resistance (ESR) is not the origin of the voltage reversion phenomenon, because the current flows through the switching path and also R_p reaches zero quickly after the switch is blocked at t_{off}, as it can be seen from Figure 3(b). R_p consumes no power when the switch is turned off.

Excluded the possibilities that the voltage reversion is caused by R_m and R_p, the major concern is focused on the equivalent parallel resistance (EPR) R_d, which represents the mechanism of dielectric loss. Since R_d is parallel to C_p, it provides a path through which the charge stored in C_p might leak internally. The charge leakage from C_p results in the voltage reversion and further magnitude reduction of v_p in the SSHI treatment.

Effective Inversion Factor

Taking the internal current leakage through the EPR R_d into consideration, in S-SSHI treatment, besides Equation (3), another relation links the voltages at the start (V_{off}) and end (V_{on}) of a switch-off interval. Mark one of the switching on maxima actions as time origin. The voltage v_p in the following half cycle is:

$$v_p(t) = V_{off} + \frac{1}{C_p}\int_0^t \left[i_{eq}(\iota) - \frac{v_p(\iota)}{R_d} \right] \mathrm{d}\iota \tag{4}$$

Since

$$v_p(T/2) = -V_{on} \tag{5}$$

where T is the period of mechanical excitation, and:

$$\frac{1}{C_p}\int_0^{T/2} i_{eq}(t)\mathrm{d}t = -2V_{oc} \tag{6}$$

[4]Since an oscilloscope probe with high input impedance (50 MΩ) is used to measure v_p in experiments, it is considered that little current leaks through the measurement process as well.

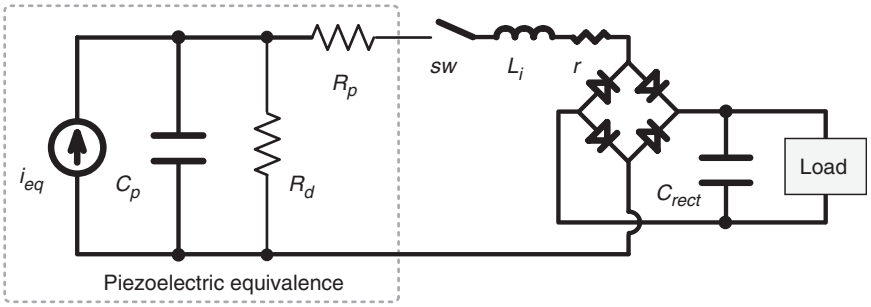

Figure 7. *Revised equivalent circuit of S-SSHI treatment.*

Substituting Equations (5) and (6) into Equation (4) at $t = T/2$ instant, we can have:

$$-V_{on} = V_{off} - 2V_{oc} - \frac{1}{R_d C_p}\int_0^{T/2} v_p(t)\mathrm{d}t \qquad (7)$$

Equation (7) can be further simplified by estimating $v_p(t)$ with its first-order approximation in this 0 to $T/2$ interval, i.e.:

$$\tilde{v}_p(t) = V_{off} - \frac{2(V_{on} + V_{off})}{T}t, \quad t \in [0, T/2] \qquad (8)$$

Substituting this approximated v_p into Equation (7) yields:

$$-V_{on} = V_{off} - 2V_{oc} - \frac{T}{4R_d C_p}(V_{off} - V_{on}) \qquad (9)$$

where V_{oc}, the open-circuit voltage can be directly measured without the SSHI circuit connected. With the two linear equations of (3) and (9), the values of V_{on} and V_{off} can be solved out.

In addition, at low excitation level, the difference between ΔV_M and $2V_{oc}$ is not significant, i.e., the effect produced by the second observed feature can be neglected, compared to that by the first one. Considering the cancellation of reversion toward inversion, the pseudo V_{off}, i.e., voltage value after the reversion, is:

$$V_{off,ps} = 2V_{oc} - V_{on} \qquad (10)$$

As illustrated in Figure 5(b), this $V_{off,ps}$ can be observed from the experimental waveform. It was taken as effective V_{off} in the previous studies. Furthermore, from Equations (3) and (9), the effective inversion factor γ_{eff} is defined as:

$$\gamma_{eff} = \frac{V_{off,ps} - V_{rect}}{V_{on} - V_{rect}} = \gamma + \frac{T}{4R_d C_p}(1 - \gamma) \qquad (11)$$

Since γ is less than 1, γ_{eff} is greater than γ. In general, the inversion effect is weakened. In Figure 3(a), it is shown that, with γ_{eff}, the calculated waveform (dash curve) approaches the experimental data quite well.[5] From Equation (3), γ approaches -1 when the quality factor of the RLC loop, i.e., Q, approaches infinity. Substituting this limit on γ to Equation (3), we can obtain the limit of the effective inversion factor as:

$$\lim_{\gamma \to -1} \gamma_{eff} = \frac{T}{2R_d C_p} - 1 \qquad (12)$$

Obviously, the effective inversion factor γ_{eff} and its limit are not only determined by the quality factor of the switching RLC loop, but also depended on the dielectric loss of the selected piezoelectric element, as well as the vibration period.

Energy Flow

To give an overall evaluation to a PEH system, not only the energy harvesting performance, but also the structural effect induced by harvesting energy from the vibrating structure are of concern (Liang and Liao, 2009; Liao and Sodano, 2009). Lesieutre et al. (2004) and Shu and Lien (2006) discussed the induced damping effect as a result of energy harvesting. Based on the analysis about the energy flow within a PEH system, Liang and Liao (2009) further pointed out that, energy harvesting is not the only function generated within the PEH system; during the harvesting process, part of energy may be dissipated in the power conditioning circuit. In addition, both energy harvesting and dissipation extract energy from the vibrating structure, and consequently bring out structural damping.

Three factors were defined by Liang and Liao (2009), in order to provide performance evaluation and comparison among the two functions of energy harvesting, energy dissipation and their effect on

[5]Detailed parameters of the experiment are provided in the next section.

structural damping. *Harvesting factor* is defined to evaluate the harvesting capability as:

$$\eta_h = \frac{E_h}{2\pi E_{\max}} \tag{13}$$

where E_h denotes the harvested energy in one cycle, $E_{\max}$ is the energy associated with vibration, multiplying by 2π to obtain the vibratory energy in one cycle. *Dissipation factor* is defined to evaluate the dissipation capability as:

$$\eta_d = \frac{E_d}{2\pi E_{\max}} \tag{14}$$

where E_d is the dissipated energy in one cycle. With Equations (13) and (14), the *loss factor* is defined as:

$$\eta_\Sigma = \frac{\Delta E}{2\pi E_{\max}} = \eta_h + \eta_d \tag{15}$$

where ΔE is the sum of E_h and E_d, which represents the total removed energy from the vibrating structure in one cycle. The loss factor is related to the capability on vibration damping, which is the combined effect of both energy harvesting and dissipation.

In order to have comprehensive studies on a certain PEH system, not only the harvesting capability, but also the side effect on energy dissipation should be taken into consideration.

With the above analysis, in an S-SSHI system, the amount of energy harvested in one cycle is:

$$E_h = 2V_{store}C_p(V_{on} - V_{off}) \tag{16}$$

The amount of energy dissipated in one cycle is:

$$E_d = C_p(V_{on} - V_{rect})^2(1-\gamma^2) + 2V_F C_p(V_{on} - V_{off}) + 2\int_0^{T/2} \frac{\tilde{v}_p(t)^2}{R_d}\,\mathrm{d}t \tag{17}$$

The three items in Equation (17) are sequentially corresponding to: the dissipation induced by the ESR of the switching path, i.e., r and R_p in series; the dissipation induced by the bridge rectifier; and the dielectric loss induced by the EPR R_d.[6]

On the other hand, in the previous studies, without considering the influence of the internal loss, the effective inversion factor was used in the calculation of the harvested and dissipated energy in one cycle with the following equations:

$$E_{h,eff} = 4C_p V_{store}(V_{oc} - V_{rect})\frac{1-\gamma_{eff}}{1+\gamma_{eff}} \tag{18}$$

$$E_{d,eff} = 4C_p(V_{oc} - V_{store})(V_{oc} - V_{rect})\frac{1-\gamma_{eff}}{1+\gamma_{eff}} \tag{19}$$

Since there is no energy return from electrical to mechanical in SSHI, all the vibratory energy is in mechanical domain. It can be calculated with the following equation:

$$E_{\max} = \frac{1-k_d^2}{2k_d^2}C_p V_{oc}^2 \tag{20}$$

where k_d^2 is the coupling coefficient of the piezoelectric device, which can be obtained from the measured resonant frequencies under open-circuit and short-circuit conditions, i.e.:

$$k_d^2 = \frac{f_{oc}^2 - f_{sc}^2}{f_{oc}^2} \tag{21}$$

where f_{oc} and f_{sc} are the open-circuit and short-circuit resonant frequencies, respectively. Substituting Equations (16)–(20) into Equations (13)–(15), the three evaluating factors can be obtained.

EXPERIMENTS

Experiments are performed, in order to measure the ERP R_d in the revised equivalent circuit, and further validate our analysis with an emphasis on energy flow.

Figure 8(a) shows the photo of the experimental setup. The main mechanical structure is a base-excited aluminum cantilever, whose excitation is from a shaker (Mini Shaker Type 4810, B & K). A piezoceramic patch of $49 \times 24 \times 0.508\,\mathrm{mm}^3$ (T120-A4E-602, Piezo System, Inc.) is bonded near the fixed end where the largest strain happens along the cantilever. Figure 8(b) illustrates the layout and dimensions of the mechanical structure. For the purpose of synchronization, an electromagnetic sensor is employed to sense the relative velocity between the cantilever end and the base. The permanent magnet acts as proof mass at the same time. It can lower the vibration frequency and increase the displacement of the free end. The output voltage from the coil, which is proportional to the end velocity, is input to a micro-controller unit (eZ430-RF2500, Texas Instrument). In the circuitry part, the micro-controller is coded to first analyze the velocity signal, and then generate switching command to drive two MOSFETs as the bi-directional switch to perform

[6]For simplicity, the first-order approximation of $v_p(t)$ is also used to estimate the dissipated energy here.

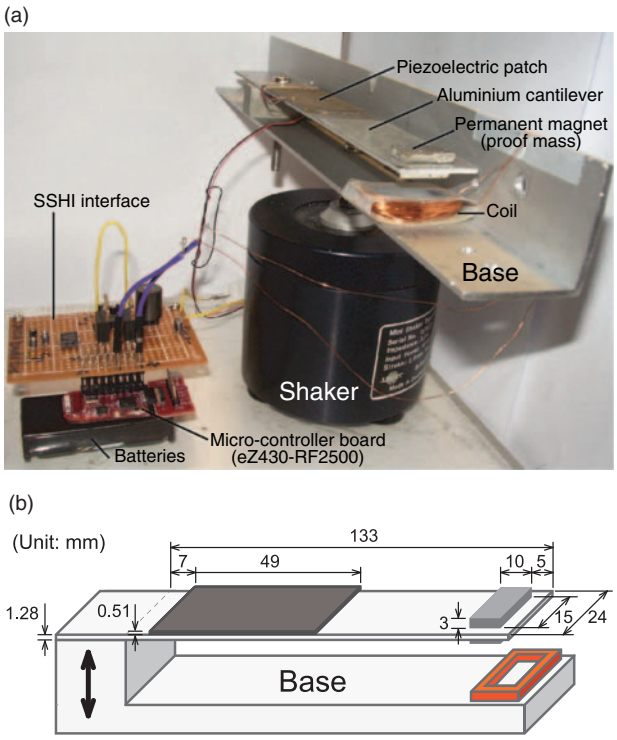

Figure 8. *Experimental setup: (a) photo of the setup and (b) layout and dimensions of the mechanical structure.*

synchronized switching actions. Although the micro-controller is powered by batteries, there are two advantages for this setup, compared to those which were commonly used in the previous studies (Guyomar et al., 2005; Lefeuvre et al., 2006). By adopting the electromagnetic velocity sensor, rather than inductive displacement sensor, self-powered sensing is achieved. Meanwhile, since the velocity signal is obtained directly, zero-crossing detection rather than peak detection is required, which might help to save some computing effort. By equipping with a micro-controller unit, which works independently and provides accesses to many peripheral devices, e.g., sensors, RF unit, and power management unit, we are getting closer toward the goal of constructing an intelligent autonomous device.

Table 1 gives some parameters of the experimental setup, including mechanical structure, interface circuitry, as well as the excitation.

Measurement of Parameters

The measurement on dielectric loss under high-power operation is an issue. The loss is non-linear, and it increases significantly under high-power operation (Hirose et al., 1993; Umeda et al., 1998). In this analysis, a linear resistance R_d is used to approximately model the influence of dielectric loss. To determine the value of R_d, the voltages of V_{on} and V_{off} under different rectified voltage V_{rect} are measured first. Since R_d is related to the theoretical V_{on} and V_{off} with Equations (3) and (9), the value of R_d can be obtained simultaneously by fitting the measured V_{on} and V_{off} data with the least square method.

Table 1. Parameters of the experimental setup.

Component	Value or model
Open circuit resonance frequency, f_{oc}	27.31 Hz
Short circuit resonance frequency, f_{sc}	27.06 Hz
Excitation frequency, f_0	30 Hz
Piezoelectric capacitance, C_p	34.69 nF
Filter capacitance, C_{rect}	10 μF
Inductance, L_i	47 mH
Switching component, *sw*	MOSFET (IRL510)
Bridge rectifier	DB104 (V_F=1.0 V)

The measured V_{on}, V_{off}, and $V_{off,ps}$ under different V_{rect}, as well as the fitted lines are shown in Figure 9. From the curve fitting process, the corresponding $R_d = 2.07$ MΩ. From the data shown in Figure 9, the ideal and effective inversion factors, i.e., γ and γ_{eff}, under different V_{rect} can be obtained. As shown in Figure 10, these two inversion factors are independent of the rectified voltage V_{rect}. In the following comparison, γ is -0.80, which is the average of the measured values under different V_{rect}. The effective inversion factor $\gamma_{eff} = -0.59$, which is obtained with this average γ according to Equation (11).

Results

Experiments on both functions of energy harvesting and dissipation are performed in order to check their correlation to the revised theory, which includes the influence of dielectric loss. Load resistors with different values are connected as DC load. Recording the voltage V_{store} across the load, the harvesting power can be obtained with the Joule's law. As for the energy dissipation, three parts should be measured individually. Power dissipated by the bridge rectifier is related to the harvesting. A sampling resistor is connected to the switching path to extract the root mean squared (RMS) current flowing through the path, so as to estimate the power dissipation of its ESR, i.e., the sum of r and R_p. The dissipation by R_d can be obtained with the RMS value of v_p.

For theoretical result, as Equations (16) and (17) give the harvested and dissipated energy in every vibration cycle, multiplying E_h and E_d by the excitation frequency $f_0 = 30$ Hz yields the power on energy harvesting and dissipation, i.e., P_h and P_d, as shown in Figure 11. Meanwhile, besides the absolute power, the relative indices, i.e., efficiencies on energy harvesting and dissipation toward the energy associated with vibration are also of interest. The harvesting factor η_h and dissipation

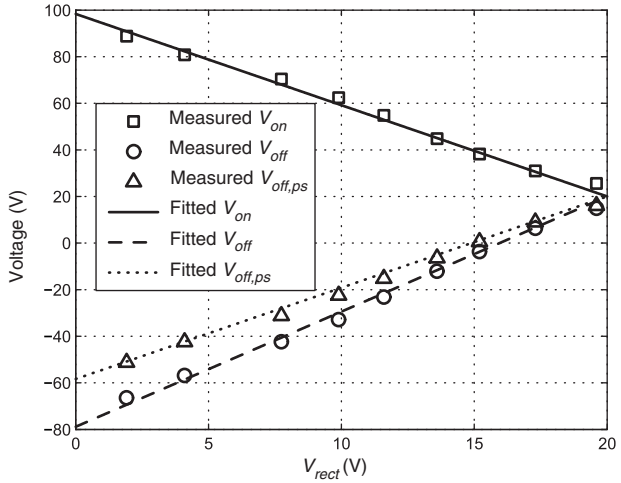

Figure 9. *Fitting the experimental data of* V_{on} *and* V_{off} *to obtain the value of* R_d.

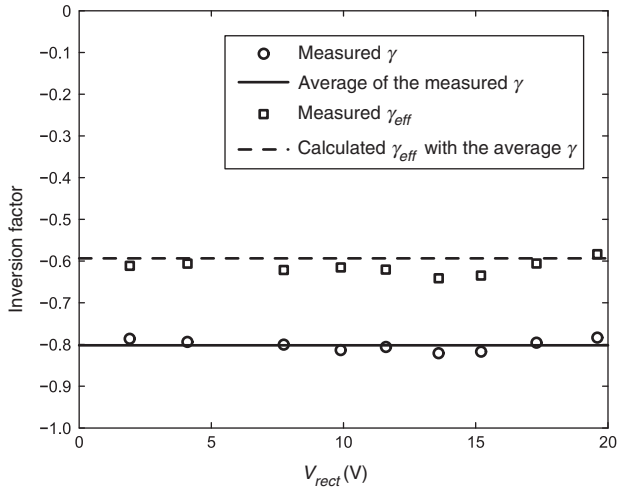

Figure 10. *Inversion factors under different rectified voltage* V_{rect}.

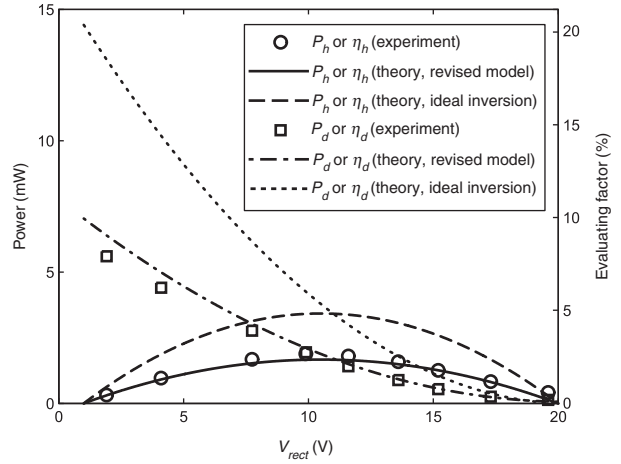

Figure 11. *Power and evaluating factors in PEH with S-SSHI interface.*

factor η_d were defined in Equations (13) and (14). In this study, since constant displacement excitation is applied,[7] the vibratory energy associated with vibration $E_{\max}$ does not change. From Equation (20), $E_{\max}$ can be derived with the coupling coefficient k_d^2, which is obtained with Equation (21). The natural frequencies under open and short circuit conditions, i.e., f_{oc} and f_{sc}, are listed in Table 1. Given that $E_{\max}$ is constant, η_h and η_d are proportional to P_h and P_d. The corresponding scale of the two evaluating factors is given by the right vertical axis in Figure 11.

Figure 11 shows that both experimental results and theoretical analyses agree with each other well. In addition, for comparison, the theoretical result with ideal inversion, i.e., assuming no reversion follows inversion, is also shown. Both predicted harvested power and dissipated power with this model are nearly 100% higher than those in real situation. Therefore, the reversion produced by dielectric loss, although small compared to the inversion, significantly degrades the efficiencies on energy harvesting and dissipation.

Besides the model validation, the results shown in Figure 11 also provide some information on the relation between energy harvesting and dissipation in S-SSHI. As we can observe from Figure 11, the harvesting power and harvesting factor attain their maxima around the middle of the V_{rect} range; for the dissipation power and dissipation factor, on the other hand, they monotonically decrease as V_{rect} increases. The trend of the harvesting factor in S-SSHI (first increase, then decrease) is similar to that in SEH and P-SSHI. However, the trend of the dissipation factor (monotonic decrease) is just opposite to that in the P-SSHI case (Liang and Liao, 2009). The loss factor η_Σ, which describes the performance of the PEH device on structural damping, was not shown in Figure 11, but it can be obtained as the sum of harvesting factor and dissipation factor.

CONCLUSIONS

In the previous theoretical analyses on PEH with SSHI interface, it was considered that, by adopting a really low loss switching inductive path, the harvesting power can be pushed toward infinity under constant displacement excitation (Lefeuvre et al., 2006). Yet, in this article, we showed that the power harvested is also much related to the transducer energy loss within the piezoelectric element, in particular, the dielectric loss. This loss causes the voltage reversion across the piezoelectric element after every inversion, weakens the inversion effect, and consequently degrades the voltage magnitude as well as the harvesting efficiency a lot. The phenomenon on voltage inversion was explained. A revised model was

[7]The relative displacement between the cantilever and the base may change when the SSHI treatment is activated. In experiment, the shaker input is adjusted to maintain the same vibration level according to the sensed velocity.

proposed to include the influence of dielectric loss in the analysis. With this model, the relation between ideal and effective inversion factor was obtained; the limit on the effective inversion factor was discussed. Theoretical results of this revised model showed good agreement with the experimental data. In addition, for overall evaluation of PEH systems, instead of merely focusing on the harvesting power, the energy flow including harvested and dissipated energy and also their corresponding evaluating factors were emphasized. The results on energy harvesting and dissipation reveal their relation under different rectified voltages in S-SSHI.

ACKNOWLEDGMENTS

The study described in this article was supported by a grant from Research Grants Council of Hong Kong Special Administrative Region, China (Project No. CUHK414809).

REFERENCES

Anton, S.R. and Sodano, H.A. 2007. "A Review of Power Harvesting Using Piezoelectric Materials (2003–2006)," *Smart Mater. Struct.*, 16:R1–R21.

Guan, M.J. and Liao, W.H. 2009. "On the Equivalent Circuit Models of Piezoelectric Ceramics," *Ferroelectrics*, 386:77–87.

Guyomar, D., Badel, A., Lefeuvre, E. and Richard, C. 2005. "Toward Energy Harvesting Using Active Materials and Conversion Improvement by Nonlinear Processing," *IEEE Trans. Ultrason. Ferroelectr. Freq. Control*, 52:584–595.

Guyomar, D., Yuse, K., Monnier, T., Petit, L., Lefeuvre, E. and Richard, C. 2006. "Semi-passive Vibration Control: Principle and Application," *Ann. Univ. Craiova, Electr. Eng. Series*, 30:57–62.

Hirose, S., Aoyagi, M. and Tomikawa, Y. 1993. "Dielectric Loss in a Piezoelectric Ceramic Transducer Under High-power Operation: Increase of Dielectric Loss and its Influence on Transducer Efficiency," *Jpn. J. Appl. Phys.*, 32:2418–2421.

Lallart, M. and Guyomar, D. 2008. "An Optimized Self-powered Switching Circuit for Non-linear Energy Harvesting with Low Voltage Output," *Smart Mater. Struct.*, 17:035030.

Lefeuvre, E., Badel, A., Richard, C., Petit, L. and Guyomar, D. 2006. "A Comparison Between Several Vibration-powered Piezoelectric Generators for Standalone Systems," *Sens. Actuators, A*, 126:405–416.

Lesieutre, G.A., Ottman, G.K. and Hofmann, H.F. 2004. "Damping as a Result of Piezoelectric Energy Harvesting," *J. Sound Vib.*, 269:991–1001.

Liang, J.R. and Liao, W.H. 2009. "Piezoelectric Energy Harvesting and Dissipation on Structural Damping," *J. Intell. Mater. Syst. Struct.*, 20:515–527.

Liao, Y. and Sodano, H.A. 2009. "Structural Effects and Energy Conversion Efficiency of Power Harvesting," *J. Intell. Mater. Syst. Struct.*, 20:505–514.

Ottman, G.K., Hofmann, H.F., Bhatt, A.C. and Lesieutre, G.A. 2002. "Adaptive Piezoelectric Energy Harvesting Circuit for Wireless Remote Power Supply," *IEEE Trans. Power Electron.*, 17:669–676.

Paradiso, J.A. and Starner, T. 2005. "Energy Scavenging for Mobile and Wireless Electronics," *IEEE Pervasive Comput.*, 4:18–27.

Richard, C., Guyomar, D., Audigier, D. and Bassaler, H. 2000. "Enhanced Semi-passive Damping Using Continuous Switching of a Piezoelectric Device on an Inductor," In: Hyde, T.T. (ed.), *Proceedings of SPIE International Symposium on Smart Structures and Materials 2000: Damping and Isolation*, 27 April, Newport Beach, USA, Vol. 3989, pp. 288–299.

Shu, Y.C. and Lien, I.C. 2006. "Efficiency of Energy Conversion for a Piezoelectric Power Harvesting System," *J. Micromech. Microeng.*, 16:2429.

Shu, Y.C., Lien, I.C. and Wu, W.J. 2007. "An Improved Analysis of the SSHI Interface in Piezoelectric Energy Harvesting," *Smart Mater. Struct.*, 16:2253–2264.

Sodano, H.A., Inman, D.J. and Park, G. 2004. "A Review of Power Harvesting From Vibration Using Piezoelectric Materials," *Shock Vib. Digest*, 36:197–205.

Umeda, M., Nakamura, K. and Ueha, S. 1998. "The Measurement of High-power Characteristics for a Piezoelectric Transducer Based on the Electrical Transient Response," *Jpn. J. Appl. Phys.*, 37:5322–5325.

Wu, W.J., Wickenheiser, A.M., Reissman, T. and Garcia, E. 2009. "Modeling and Experimental Verification of Synchronized Discharging Techniques for Boosting Power Harvesting from Piezoelectric Transducers," *Smart Mater. Struct.*, 18:055012.